An automated glitch-detection/restoration method of atomic force microscope images

Chankyeong Hyon, Sangwook Oh, Hyungkwon Kim, Sanghoon Sull, and Sungwoo Hwang[a)]
Department of Electronic and Computer Engineering, Korea University, Anam, Sungbuk, Seoul 136-075, Korea

Doyeol Ahn
Institute of Quantum Information Processing and Systems, University of Seoul, 90 Jeonnong, Tongaemoon, Seoul 130-743, Korea

Youngju Park and Eunkyu Kim
Semiconductor Materials Laboratory, Nanodevice Research Center, Korea Institute of Science and Technology, P. O. Box 131, Cheongryang, Seoul 130-650, Korea

(Received 2 April 2002; accepted for publication 27 May 2002)

An automated glitch-detection/restoration method of atomic force microscope images is proposed and implemented. Contrary to other manual methods, our method is based on the probability distribution of the derivative of the scanned image data. The glitches are identified as the points that deviate from a normal probability density function. The essence of the automation is calculating the distribution of the scanned image and removing the points that deviate from the normal distribution. Quantitative analysis of the original and the restored image have been performed and the degree of deformation of the restored images has also been analyzed. This technique can directly be applied to other types of scanning probe microscope equipments. © *2002 American Institute of Physics.* [DOI: 10.1063/1.1497503]

I. INTRODUCTION

Since the first introduction of the scanning tunneling microscope in 1981 by Binning and Rohrer,[1] scanning probes have widely been used to measure various surface properties such as topography, frictional force difference, electrostatic potential, capacitance, magnetic force, temperature, etc. These nanoprobing techniques have become common for qualitative and/or quantitative analyses of virtually all kinds of samples, and thus have brought in a wide spectrum of scanning probe microscopies (SPMs).[2] Despite some drawbacks, such as tip-shape dependence of the image or nonideal response of the piezoscanner, the atomic force microscope (AFM) is the most versatile piece of equipment among the microscopes, allowing the three-dimensional reconstruction of the sample topography with atomic resolution. The versatility comes from the fact that there is no restriction on the material to be imaged using this microscopy technique. Liquid materials as well as solids can be imaged, and even biological cells can be observed by the AFM.[3,4]

Although the SPM can image the sample surface with atomic resolution, different types of distortion are introduced during the measurement. The most common of these is the distortion due to the tilt of samples and probes. In-depth analyses and modeling on this matter have been successfully carried out by Yurov *et al.* and others.[5,6] The thermal drift of the tip with respect to the sample, and the nonlinear response of the piezoscanner have been extensively investigated.[5] Furthermore, automatic calibration methods have provided successful on-line image correction.[5,7,8] The convolution effect of the tip is another source of the distortion, which becomes pronounced when measuring structures with high aspect ratios, or when measuring ultrasmall features. Methods to obtain deconvoluted images are currently being investigated by many groups.[9,10] Inherent distortions due to streaks are easily observed, for example, in patterned surfaces. A mathematical model for the generation of the streaks and a removing algorithm applying adaptive notch filtering have been investigated by Yu *et al.*[11] The feedback circuit and the external noise sources also introduce the spatial frequency noise, which can be partly removed by using fast Fourier transform filtering.[12] All of those distortions prevent the proper analysis and interpretation of the obtained SPM data. Nevertheless, the introduction of modern signal processing techniques supported by powerful computers have been creating a method of reconstructing the real surface image from a distorted image.

Glitches are often observed while taking AFM images, and they persist even after applying the filters introduced above. Furthermore, only superficial and limited understanding about the generation of glitches exists and there rarely is a generally known algorithm to adequately handle images with glitch. Some manufacturers provide manual glitch removal software based on the median filtering method,[12] but the detection of the glitch is time consuming and depends solely on the user's data point by data point decision.

In this article, the properties of the glitch are analyzed, the AFM image data with glitches are formulated using a mathematical model, and then a detection algorithm is pro-

[a)]Author to whom correspondence should be addressed: also at *iQUIPS.*

posed. The proposed algorithm is based on the probability density function of the spatial derivative of the height data. The glitches are identified as the points that are far away from the mean of the probability density function since the derivative value is large at the glitch points. The essence of the automation is calculating the distribution of the scanned image and removing the points that are deviated from the normal distribution. Finally, the proposed glitch-detection/restoration is applied to original AFM images with glitches and the restored images are quantitatively compared with the original images to ascertain the effectiveness of the algorithm.

II. GLITCH DETECTION AND RESTORATION SCHEME

A. General aspects of atomic force microscopy images

The AFM generally images the topography of sample surfaces with respect to a scan coordinate system (SCS). The probe is raster-scanned parallel to the *x*-*y* plane of the SCS while maintaining the contact force between the sample and the probe to a set point by relying on an electronic feedback system. The variation in the *z* direction, which corresponds to the height data, is monitored and stored at each particular sampling point (x,y).[6] The scanning direction can be either horizontal (x) or vertical (y). Images of 256×256 pixels are usually obtained.

Since the glitch gives sudden variation of the height data, the quantitative measure of the glitch generation will be the derivative of the height data. The distribution of the derivative of the height data could be approximated by several different types of functions. We find that usual semiconductor surfaces can be approximated by the Gaussian distribution. Figure 1 shows three different AFM images of semiconductor surfaces without glitches. Figures 1(a), 1(b), and 1(c) are the surface images of a GaAs substrate, a *p*-type silicon substrate, and a SiO_2 substrate, respectively. Figures 1(d), 1(e), and 1(f) show the probability distribution of the spatial derivative of their height data $H'_T(x,y)$. (The detailed definition will be given in Sec. II C.) Note that the distributions are plotted in the log scale. The solid lines denote the results of fitting the probability distribution with the Gaussian distribution. The fitting error is smaller than 0.2%. The results suggest many semiconductor surfaces can be approximated by the Gaussian distribution function. The root-mean-square (rms) roughness values of three cases are 0.248, 0.127, and 0.16 nm. The standard deviation values of the distribution functions are 1.07, 0.40, and 0.45 nm, respectively. One important thing to note is that the rms roughness is almost proportional to the standard deviation.

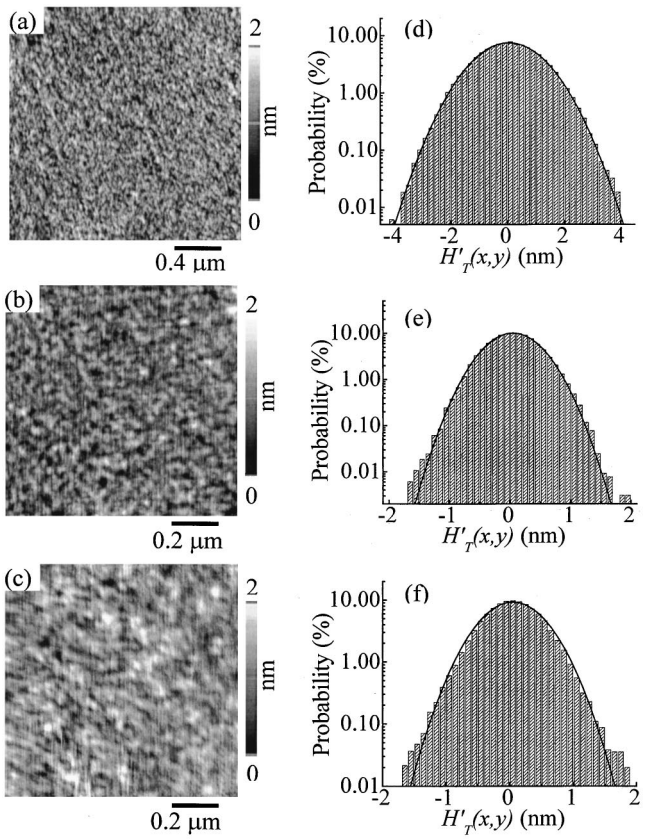

FIG. 1. AFM images of (a) a GaAs substrate, (b) a *p*-type silicon substrate, and (c) a SiO_2 substrate. Corresponding distribution functions are shown in (d), (e), and (f), respectively.

B. Properties of glitches

The most frequent source of the glitch is the existence of moving particles, which drastically change the height of the probe. Once a sudden change of the probe height occurs, it persists during the scanning of even an entire line. The existence of the moving particle could be considered to be real but the glitch line behind the particle is an unwanted artifact. Glitches are also observed in samples with rough surfaces. In this case, the piezoscanner cannot follow drastic changes of the sample surface in the *z* direction, when the feedback parameters are adjusted for surfaces with a small degree of roughness. The feedback parameter can be set to prevent the generation of the glitch but this may cause distortion of the original surface image.

Figure 2(a) shows an example of an AFM image with glitches, which is obtained from a reactive-ion-etched (100) GaAs sample. The sample surface treated by the reactive ion etching becomes comparatively rough or corrugated, and residual particles are frequently present. Therefore, the glitch generation becomes more probable than on clean bare GaAs surfaces. The image was scanned in the *y* direction and the vertical bright or dark lines are identified as glitches, where a drastic change in the height is exhibited as an abrupt brightness change. It can also be seen that glitches are generated consecutively, forming double or triple glitch lines, which makes direct filtering of the raw data difficult. More detailed aspects of the glitches can be observed in the height profile analysis [Fig. 2(b)] along the line depicted in Fig. 2(a). The *y* coordinate is fixed at 246, while the *x* coordinate varies from 219 to 256. The distance between the sampling points is 19.53 nm. Seven glitches are clearly identified as the points of negative height values.

The height profile analysis of Fig. 2(b) clearly suggests that the derivative of the height with respect to the scan position at glitch points will be much larger than the derivatives at normal positions. Therefore, the existence of the

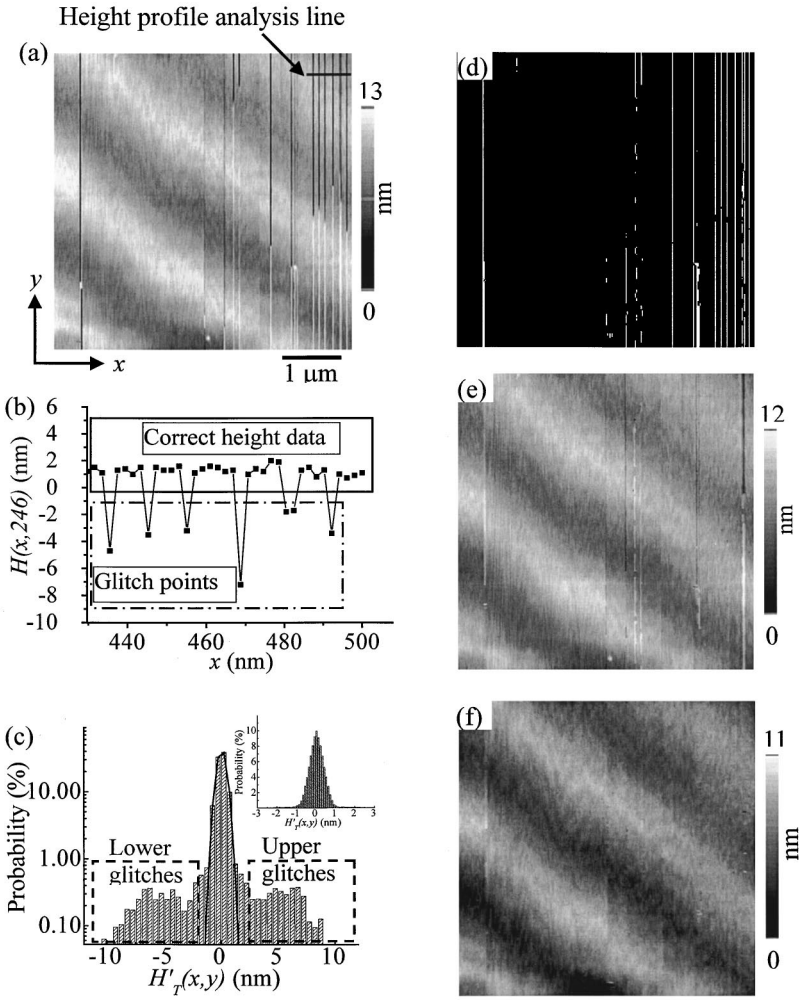

FIG. 2. (a) An example of the AFM image with glitches obtained from a reactive-ion-etched (100) GaAs sample, and (b) the height profile analysis result along the line depicted in (a). (c) The probability distribution of $H'_T(x,y)$, (d) the detected glitch image, (e) the restored image, and (f) the restored image after the second detection/restoration process.

glitch will deviate corresponding data points that are originally fit in the usual Gaussian distribution. Figure 2(c) shows the logarithmic probability distribution of the image shown in Fig. 2(a). We can identify many data points that have large derivative values and lie outside the original Gaussian distribution without any glitch point (the solid line). If the number of glitch data points is much smaller than the total number of data points, we can still find out the original distribution utilizing only the normal points with small derivative values. The key aspect of our automatic glitch-detection algorithm thus is calculating the Gaussian distribution and identifying glitches from the distribution.

C. Formulation of atomic force microscopy image data with glitches

A mathematical model of the AFM image data with glitches can be formulated as follows:

(1) Let H be square image data with $N\times N$ pixels. The height of each pixel is represented by $H(x,y)$, where $x,y=1,2,\ldots,N$. For convenience, the direction of the AFM scanning is defined to be the y direction.

(2) Define the derivative of the height data along a direction perpendicular to the scan direction (in the x direction); $H'_T(x,y)=\partial H(x,y)/\partial x$, for each y. Since we treat x and y as integers, the unit of $H'_T(x,y)$ is nm.

(3) Assume that $H'_T(x,y)$ is real and random.

(4) Define the probability of the derivative value as $F_T(r)$;

$$F_T(r)=\Pr[q(r-1)<H'_T(x,y)\leqslant q(r)|q(r)\equiv cr,c=\text{constant}],$$

where c is an empirical quantization constant and r is the random variable used for obtaining the distributional property of $H'_T(x,y)$. Then the probability density function (PDF) of $H'_T(x,y)$ can be defined as $f_T(r)=dF_T(r)/dr$.

(5) If the function $F_T(r)$ is assumed as a Gaussian distribution, as suggested in Sec. II A, then the PDF $f_T(r)$ has the form

$$f_T(r)\approx 1/\sqrt{2\pi\sigma_T^2}e^{-(r-a_T)^2/2\sigma_T^2},$$

where α_T is the mean value near zero and σ_T is the standard deviation depending on the surface roughness.

(6) Since the value of $H'_T(x,y)$ at the glitch will be much larger than the value at normal surfaces, threshold detection can be applied. A possible threshold for the glitch will then be $\mathrm{Th}_T^{\pm}=\alpha_T\pm\sigma_T$.

(7) The glitch is generated as a line along the scanning direction. When a glitch is generated, $H(x,y)$ is maintained at the same value along the line. This means that the deriva-

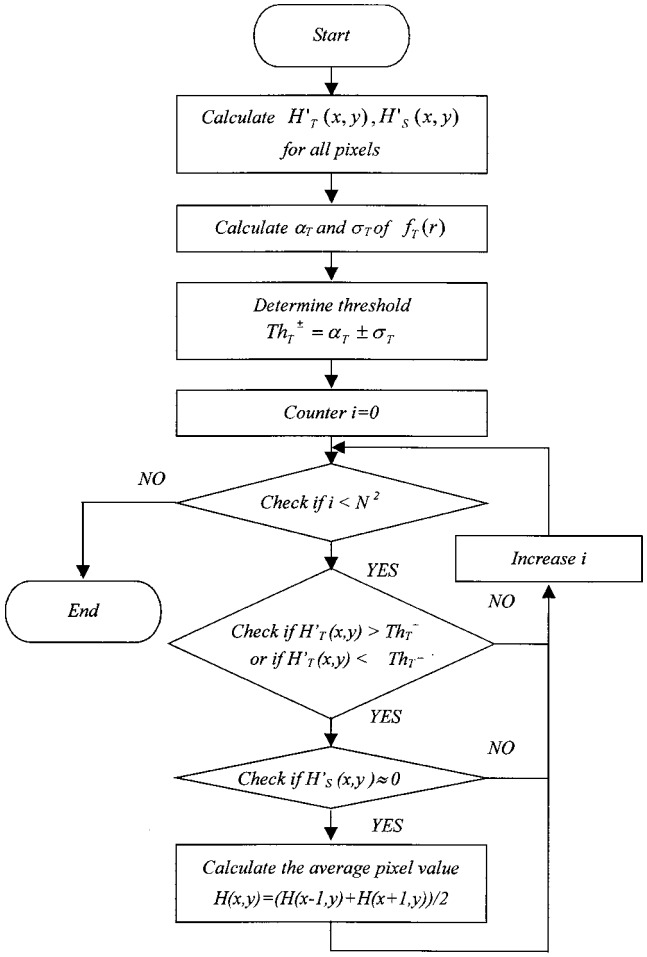

FIG. 3. Flowchart of the proposed glitch-detection/restoration algorithm.

tive of the glitch in the scanning direction is almost zero. In other words, $H'_S(x,y) \approx 0$ where S represents the derivative in the AFM scanning direction.

D. Detection and data restoration algorithm of glitches

Based on the above formulation of the image data, we rely on the density function of the derivative to detect the glitch and restore the real image. The developed algorithm follows the steps given below.

(1) Calculate the derivative $H'_T(x,y)$ and $H'_S(x,y)$ for all the pixels.

(2) Calculate $f_T(r)$.

(3) Calculate the mean α_T and the standard deviation σ_T of $f_T(r)$.

(4) Determine the upper and the lower threshold value $\mathrm{Th}_T^{\pm} = \alpha_T \pm \sigma_T$.

(5) For the pixels of step (1), check the pixel (x,y) as a glitch candidate if $H'_T(x,y) > \mathrm{Th}_T^+$ or $H'_T(x,y) < \mathrm{Th}_T^-$.

(6) For each glitch candidate pixel, check if $H'_S(x,y) \approx 0$. If so, this pixel is determined as the glitch.

(7) At the glitch pixel, calculate the average pixel value $H(x,y) = [H(x-1,y) + H(x+1,y)]/2$ from the left and the right pixel values.

Note that, in step (1), the first line of the pixel is assumed to contain the correct values. In step (4), the upper and the lower threshold values are needed to filter out bright or dark glitches, respectively. The calculated PDF in step (2) should be as similar as possible to the PDF of the image with no glitches. Therefore, a rough window for the fitting is needed. In Sec. II A, it is shown that the rms roughness is proportional to the standard deviation of the distribution. Furthermore, the existence of the glitch is not expected to change the rms roughness to a large extent. The window can be set as integer multiples of the virtual standard deviation

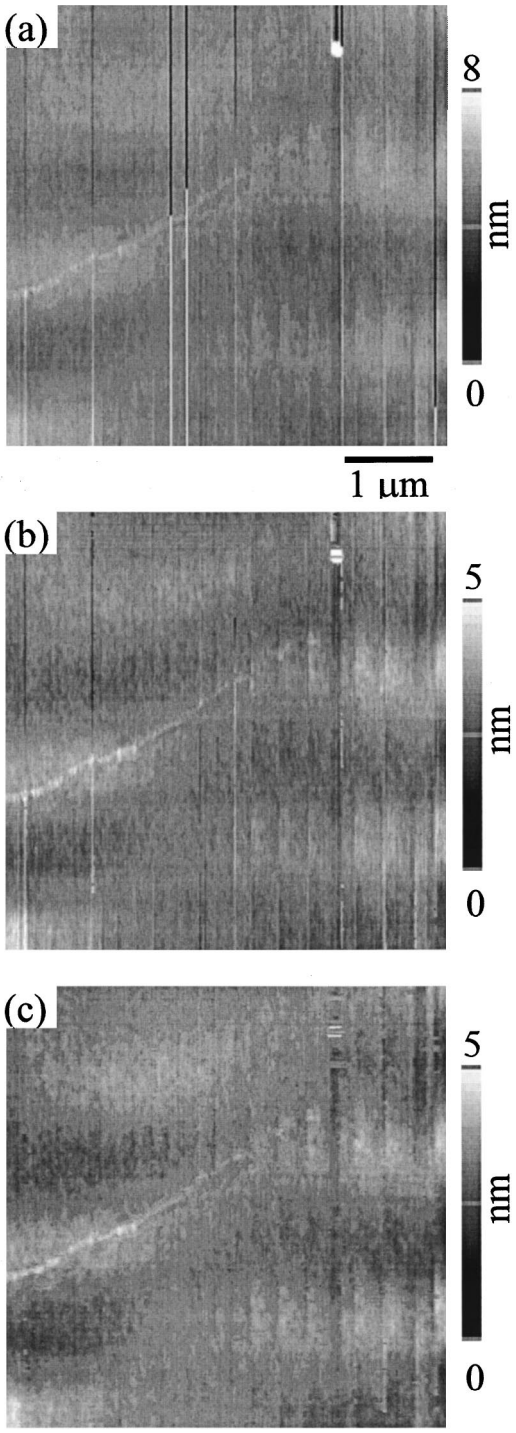

FIG. 4. Glitch removal of a smooth surface image: (a) the original image with glitches, (b) the restored image after the first removal process, and (c) the restored image after the second removal process.

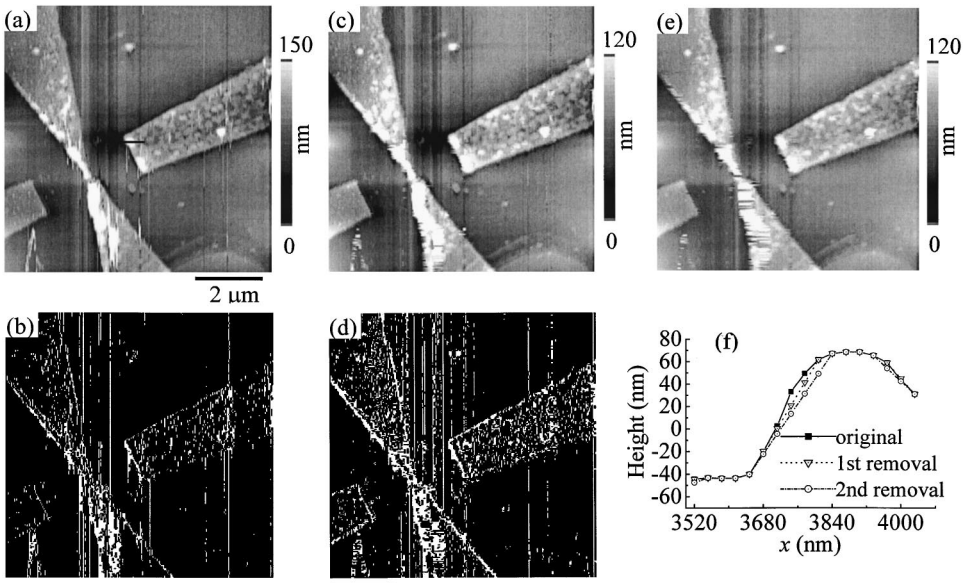

FIG. 5. Difficulties in detecting glitches when glitches are present with sharp-edged patterns: (a) the original AFM image of the metal electrode patterns with sharp edges, (b) the glitch image derived from the first glitch detection, (c) the partly restored image, (d) the glitch image derived from the second glitch detection, (e) the glitch removed and partly corrupted final image, and (f) the height profile analysis along the line depicted in (a).

estimated from the rms roughness. In step (7), the first-order approximation is used and real height data are recovered by averaging two height data adjacent to the glitch point. The above algorithm is summarized in the flowchart of Fig. 3.

III. EXPERIMENTAL RESULTS AND DISCUSSIONS

We used AFM data obtained from a commercially available AFM.[12] The glitch detection and restoration algorithm was coded in C language and a common PC was used for the data processing. Since most of modern AFMs use PCs for the probe control and image processing, our implementation can be directly applicable to them. Three different AFM images will be discussed. Prior to the glitch detection, the original data went through the tilt correction and flattening process. All images have the same scale in the x and the y directions, and the scanning direction is y. The scales in the z direction are set to display the height data of the whole plane.

First of all, the image of Fig. 2(a) has gone through the developed detection/restoration algorithm. Figure 2(c) shows the PDF obtained from the image. The calculated α_T and σ_T of the $H'_T(x,y)$ function were 0.000 156 and 2.244 241 nm, respectively. The upper and lower thresholds $\mathrm{Th}_T^{\pm}$ determined from α_T and σ_T were 2.244 398 and 2.244 085 nm, respectively. The dotted squares on both sides of Fig. 2(c) correspond to the glitches identified by applying the calculated $\mathrm{Th}_T^{\pm}$ values. The inset shows the same distribution in a linear scale, where the Gaussian distribution is more evident. Figure 2(d) shows white lines detected as glitches. Approximately 10 lines are determined as glitches, while 16 glitch lines are discernible to the naked eye as shown in Fig. 2(a). Figure 2(e) shows the restored image after removing the detected glitches. All of the 10 detected glitches are removed while 6 undetected glitches still exist.

Generally, two detection and restoration steps are sufficient to completely remove glitches for the samples tested in this work. Figure 2(f) exhibits the image of Fig. 2(e) after going through second glitch removal processes. As is shown in the above paragraph, more than 60% of the glitches are removed in the first detection and restoration process, and the remaining glitches are almost completely removed after the second process. The rms roughness value can be a figure of merit in the detection and restoration process, since glitches exaggerate the rms roughness value. The original image of Fig. 2(a) has the rms roughness value of 2.24 nm,

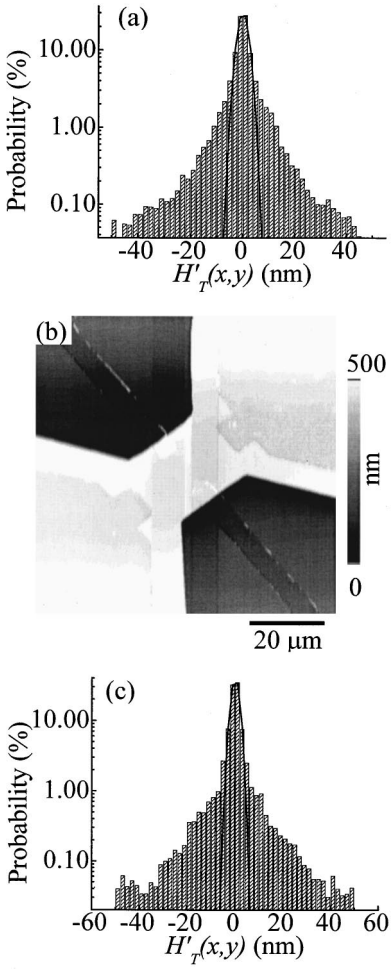

FIG. 6. (a) The PDF of the image shown in Fig. 5(a). (b) The image of a wet etched GaAs pattern and (c) its PDF.

which is comparable with the rms roughness of 3.6 nm obtained from an electron cyclotron resonance plasma etched GaAs sample.[13] The rms roughness values of Figs. 2(e) and 2(f) are 1.60 and 1.56 nm, respectively. The difference between the rms roughness values of the original and the restored images is about 29%.

The next case considered in this study is shown in Fig. 4(a). This image is obtained from a relatively smooth semi-insulating GaAs wafer. Several corrugations and eight glitch lines are observed in the original image. Two steps of glitch detection and restoration were performed and the results of each restoration step are shown in Figs. 4(b) and 4(c), respectively. As shown in Fig. 4(b), only one-half of the glitches are removed in the first detection and restoration process. The calculated α_T and σ_T were 0.000 115 and 1.170 735 nm, respectively. The upper and lower thresholds $\mathrm{Th}_T^{\pm}$ were 1.170 850 and $-1.170\,620$ nm, respectively. The result of the second detection and removal process is shown in Fig. 4(c). In this case, calculated α_T and σ_T were 0.000 115 and 0.269 952 nm, respectively. The upper and lower thresholds $\mathrm{Th}_T^{\pm}$ determined from α_T and σ_T, were 0.269 837 and $-0.270\,067$ nm, respectively. It is clear that the glitches are removed almost completely. The glitch removal becomes more important when considering the rms roughness values of smooth surfaces. The rms roughness of Fig. 4(a) is 1.080 nm, while those of Figs. 4(b) and 4(c) are 0.573 and 0.407 nm, respectively. The differences in the rms roughness values between the original and the restored images are 47% and 62%, respectively.

The final case considered in this study is shown in Fig. 5(a). Four metal electrodes, 100 nm in height, were fabricated on a silicon substrate by electron beam lithography and lift-off process.[14] This image is chosen with the intention of testing the ability of the developed algorithm when the glitches are mixed with patterns. Huge height changes along the edge of the metal electrodes will be detected as glitches by the proposed algorithm. The calculated α_T and σ_T of $H_T'(x,y)$ were 0.000 044 and 9.882 535 nm, respectively. The upper and lower thresholds, $\mathrm{Th}_T^{\pm}$, were $-9.882\,979$ and 9.882 091 nm, respectively. Figure 5(b) shows the glitches detected when applying the calculated threshold. Some parts of the edge of metal electrodes, as well as the real glitches, are determined as glitches. The glitch removal result is shown in Fig. 5(c). Approximately five out of the ten glitches discernible to the naked eye are removed but the rest remain. Figure 5(d) shows the glitch image of the second removal process, where most of the glitch lines are detected correctly. The restored image in Fig. 5(e) shows that the glitch lines are almost completely removed while it can be noticed that there is a slight change in some of the metal regions.

Figure 5(f) shows the height profile analysis results along the thick solid line marked in Fig. 5(a). The filled squares are data points of the original image and the open symbols are the data points after the first and the second glitch removal processes. It is clearly noted that the glitch removal processes erroneously decrease the slope of the metal edge (approximately 33%). This decrease in the slope decreases the contrast of the image.

Figure 6(a) shows the PDF of the patterned surface of Fig. 5(a). Figure 6(b) shows the image of a mesa etched GaAs substrate without any glitch and Fig. 6(c) shows its PDF. The solid lines in Figs. 6(a) and 6(c) denote the fitting results obtained from our algorithm. There are data points with large derivative values in Fig. 6(c) and they are originated from the pattern edges as well as from the glitches. Figure 6(c) more clearly shows that many of the data points with large derivative in Fig. 6(a) are originated from the pattern edges.

More advanced glitch-detection/restoration algorithms for the patterned images should be the two-dimensional partitioning of the image by selecting areas of similar height and applying the proposed algorithm separately. The main idea of the one-dimensional algorithm remains the same. Finally, we should emphasize that the glitch detection and restoration implemented in the above examples are automated and any type of manual handling is not involved. The algorithm can also be applied to other SPM images other than AFM.

ACKNOWLEDGMENTS

This work was supported by the Korean Ministry of Science and Technology through the Creative Research Initiatives Program under Contract No. M1-0116-00-0008. The work at KIST was supported by the KRCF project on quantum dots functional devices with Contract No. 2N22850 and QSRC program at Dongguk University. The work at Korea University was supported by the Brain Korea 21 project in 2001.

[1] G. Binnig, H. Rohrer, CH. Gerber, and E. Weibel, Phys. Rev. Lett. **49**, 57 (1982).
[2] Roland Wiesendanger, *Scanning Probe Microscopy and Spectroscopy* (Cambridge University Press, Cambridge, 1994).
[3] P. K. Hansma, J. P. Cleaveland, M. Radmacher, D. A. Walters, P. E. Hillner, M. Bezanilla, M. Fritz, D. Vie, H. G. Hansma, C. B. Frater, J. Massie, L. Fukunaga, J. Gurley, and V. Elings, Appl. Phys. Lett. **66**, 1738 (1994).
[4] H. Muramatsu, N. Chiba, K. Homma, K. Nakajima, T. Ataka, S. Ohta, A. Kusumi, and M. Fujihira, Appl. Phys. Lett. **66**, 3245 (1995).
[5] V. Yu. Yurov and A. N. Klimov, Rev. Sci. Instrum. **65**, 1551 (1994).
[6] G. S. Pingali and R. Jain, Proceedings of the Instrumentation and Measurement Technology Conference, May 1993, p. 327.
[7] R. C. Barrett and C. F. Quate, Rev. Sci. Instrum. **62**, 1393 (1991).
[8] G. A. G. Cidade, G. Weissmuller, and P. M. Bisch, Rev. Sci. Instrum. **69**, 3593 (1998).
[9] P. Markiewicz and M. C. Goh, Rev. Sci. Instrum. **66**, 3186 (1995).
[10] S. I. Park, Proceedings of the 1st Korea–U.S.–Japan Workshop on Nanostructure Science and Technology, 2-2.
[11] T. H. Yu and S. K. Mitra, Proceedings of the International Symposium on Speech, Image Processing and Neural Networks, 1994, p. 784.
[12] Autoprobe CP, Park Scientific Instruments.
[13] S. F. Yoon, T. K. Ng, and H. Q. Zheng, Mater. Sci. Semicond. Process. **3**, 207 (2000).
[14] S. K. Jung, C. K. Hyon, J. H. Park, S. W. Hwang, D. Ahn, M. H. Son, B. D. Min, Yong Kim, and E. K. Kim, Appl. Phys. Lett. **75**, 1167 (1999).